

# All-Polymer Fiber Organic Electrochemical Transistor for Chronic Chemical Detection in the Brain

Jianyou Feng, Yuan Fang, Chuang Wang, Chuanrui Chen, Chengqiang Tang, Yue Guo, Liyuan Wang, Yiqing Yang, Kailin Zhang, Jiajia Wang, Jiawei Chen, Xuemei Sun,\* and Huisheng Peng\*

Continuous and precise monitoring of chemicals in the brain can assist in understanding the working mechanism of the brain and exploring therapeutics for nerve disorders. Organic electrochemical transistors (OECTs) are employed for this purpose due to their high sensitivity from the in situ amplification effect. However, the chronic and stable detection of chemicals in the brain is rarely reported for OECTs. It is possibly due to the chronic inflammation from mechanical mismatch between the device and soft brain tissue as well as the biofouling that hinder the diffusion of chemicals to decrease the sensitivity similar to other implanted devices. Therefore, an all-polymer fiber OECT (PF-OECT) is designed, composed solely of conductive polymers and fluorine rubber. The PF-OECT shows matching modulus with the soft brain tissue and good anti-biofouling performance. It also demonstrates both high sensitivity and electrochemical stability under dynamic deformations and in complex protein solutions. Finally, the PF-OECT is implanted into the mouse brain, achieving a stable 14-day ascorbic acid monitoring. The design strategy of PF-OECT presents a potential avenue for developing more biomedical devices.

sensitive electrochemical sensors.<sup>[4]</sup> They have also been widely used for chemical sensing in vitro and in vivo.<sup>[5]</sup>

However, most of the currently reported OECTs are difficult to realize long-term monitoring of chemicals in vivo. The possible reasons are as follows. First, the current implantable OECTs for chemical sensing mostly depend on rigid metal and carbon fiber electrodes, which display mismatched mechanical properties with the soft brain tissue.<sup>[6]</sup> This will cause tissue damage and inflammation around the devices due to the micromotion between them two.<sup>[7]</sup> Second, biofouling such as protein corona formation on the electrode surface after implantation hinders the diffusion of chemicals, causing a decrease in sensitivity and thus inaccurate results.<sup>[8]</sup> The protein adhesion around the probe is mainly determined by the surface properties of sensing electrode, especially hydrophilicity.<sup>[9]</sup> For this reason, soft devices


without proper surface design may still cause protein adhesion.<sup>[10]</sup> Although some anti-biofouling methods have been developed, most of them are based on surface modifications with hydrophilic coatings, which may reduce the active surface areas of the electrochemical sensors to decrease the sensitivity.<sup>[9a,11]</sup>

Here, we introduce an all-polymer fiber OECT (PF-OECT) to address the above issues. The poly(3,4-ethylene dioxathiophene):poly(styrene sulfonate) (PEDOT:PSS) fiber was chosen as the main components of all the electrodes and channels, and fluorine rubber was used as an insulating layer. The PF-OECT showed a Young's modulus similar to that of the soft brain tissue, as well as good anti-biofouling performance due to the high hydrophilicity of PEDOT:PSS fibers (P-fibers). As a proof of concept, the PF-OECT was used to detect ascorbic acid (AA) with a high sensitivity of  $0.587 \pm 0.017 \text{ mA (lg([AA] M}^{-1})^{-1})^{-1}$  and achieved stable 14-day detection in the mouse brain.

## 1. Introduction

The chronic monitoring of chemicals in the brain is essential for exploring the working mechanism of the brain and developing therapeutic strategies for neural system diseases.<sup>[1]</sup> Electrochemical sensors are easily miniaturized for implantation and have been widely used in vivo.<sup>[2]</sup> One of the key requirements for monitoring is high sensitivity, as very small variations in the concentrations of certain chemicals may lead to noticeable changes in brain function.<sup>[3]</sup> Organic electrochemical transistors (OECTs) with three terminals, due to their in situ amplification effect, offer a promising strategy for highly

J. Feng, Y. Fang, C. Wang, C. Chen, C. Tang, Y. Guo, L. Wang, Y. Yang, K. Zhang, J. Wang, J. Chen, X. Sun, H. Peng  
State Key Laboratory of Molecular Engineering of Polymers  
Department of Macromolecular Science and Laboratory of Advanced Materials  
Fudan University  
Shanghai 200438, China  
E-mail: sunxm@fudan.edu.cn; penghs@fudan.edu.cn

 The ORCID identification number(s) for the author(s) of this article can be found under <https://doi.org/10.1002/adfm.202214945>.

DOI: 10.1002/adfm.202214945

## 2. Results and Discussion

### 2.1. Design and Fabrication of PF-OECT

PEDOT:PSS was chosen to fabricate the fiber electrode because of its high biocompatibility, conductivity and extrusion

processability into fibers.<sup>[12]</sup> Previously, most PEDOT:PSS fibers were pursued with high conductivity, while resulting in poor softness and hydrophilicity.<sup>[12,13]</sup> Here, we balanced the conductivity, softness and hydrophilicity of the fibers by introducing dimethyl sulfoxide (DMSO) and dodecylbenzene sulfonic acid (DBSA) into the pristine PEDOT:PSS solution for extruding. DMSO was used to increase the conductivity of PEDOT:PSS as the secondary dopants.<sup>[14]</sup> DBSA was used to induce the physical cross-linking of PEDOT chains<sup>[15]</sup> to promote gelation from solution. The content of DBSA was changed to regulate the formability and properties of the fibers (Figure S1, Supporting Information). Without DBSA or its amount lower than 3 v/v%, PEDOT:PSS solution could not form gel fiber. When the amount of DBSA was higher than 5 v/v%, it was too fast for the gel formation to be extruded into fiber. Therefore, the amount of DBSA was optimized to be 3.5 v/v%.

Then the PEDOT:PSS solution containing of DMSO and DBSA was extruded as the core along with the sodium alginate solution as the sheath through a three-channel spinneret (Figure S2, Supporting Information). Sodium alginate coagulated quickly when it was extruded into the calcium ions solution, which would endow enough time for the PEDOT:PSS spontaneous gelation. The Reynolds number of both solutions was controlled below 1 for the laminar flow during extrusion to guarantee their stable interfaces (Figure S3, Supporting Information).<sup>[16]</sup> Then, the P-fibers were separated from the

calcium ions cross-linked alginate hydrogel and dried at room temperature.

The diameters of P-fibers shrunk from  $342 \pm 30$  to  $44.8 \pm 3.6 \mu\text{m}$  during the drying process and swelled to  $82.5 \pm 8.2 \mu\text{m}$  after immersing in water for 5 min (Figure 1a–e; Figure S4, Supporting Information). The P-fibers were insulated with fluorine rubber with the assistance of stereotaxic apparatus under microscope, where the lengths of the channel and gate were carefully controlled to 2 and 1 mm, respectively. Finally, PF-OECT was obtained through folding up a P-fiber with two insulated ends and a channel in the middle, and paralleling with another insulated P-fiber with one end as a gate electrode (Figure S5, Supporting Information).

The component of the P-fiber was studied by X-ray photoelectron spectroscopy (XPS) and Raman spectra (Figure S6, Supporting Information). The XPS spectra showed that the insulating PSS was partially removed compared with pristine PEDOT:PSS, which was in favor of the increasing conductivity for P-fibers.<sup>[18]</sup> The reservation of some PSS could ensure the high hydrophilicity and softness of P-fibers. In addition, Raman spectra showed a red-shift of the symmetrical  $C_{\alpha} = C_{\beta}$  stretching vibration of P-fibers compared to the pristine PEDOT:PSS, illustrating the resonant structure transformation of PEDOT chain from benzoid to quinoid, which was also beneficial to high conductivity.<sup>[19]</sup> As a result, the P-fibers showed conductivities of  $231.3 \pm 21.5 \text{ S cm}^{-1}$ , which are comparable to the previously reported PEDOT materials.<sup>[20]</sup>

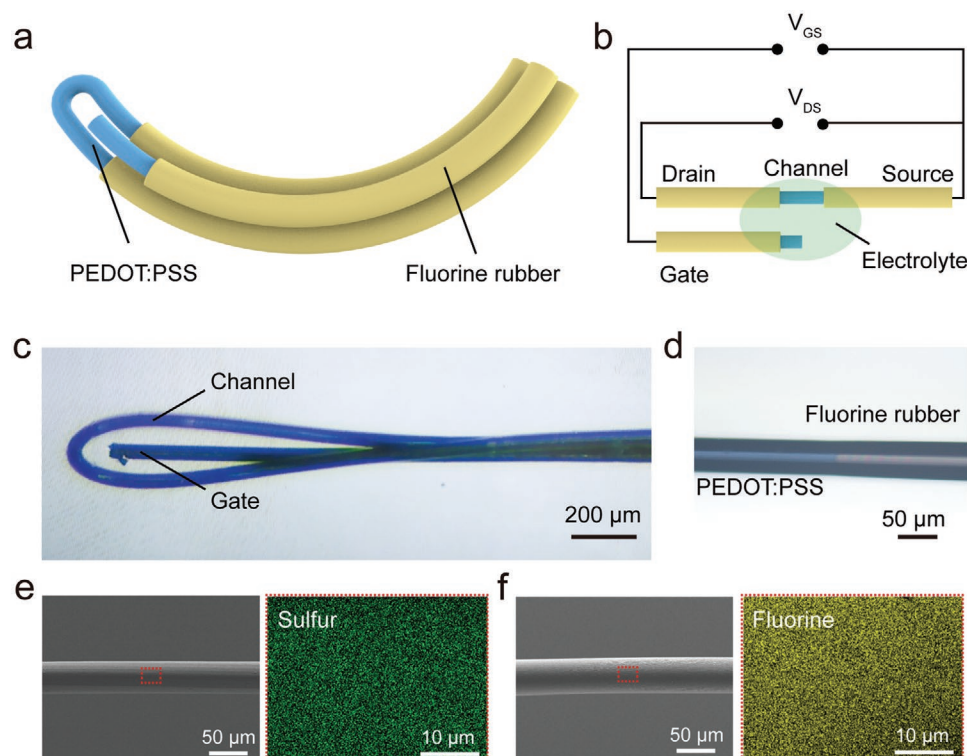


**Figure 1.** Schematic diagram and structural characterization of the PF-OECT. a,b) Schematic illustration and circuit diagram of the PF-OECT. c) Photograph of a PF-OECT. d) Photograph of a fluorine rubber insulated P-fiber for gate. e) Scanning electron microscopy image of a P-fiber and the energy dispersive mapping of sulfur element in P-fiber. f) Scanning electron microscopy image of a fluorine rubber insulated P-fiber and the energy dispersive mapping of fluorine element in fluorine rubber.

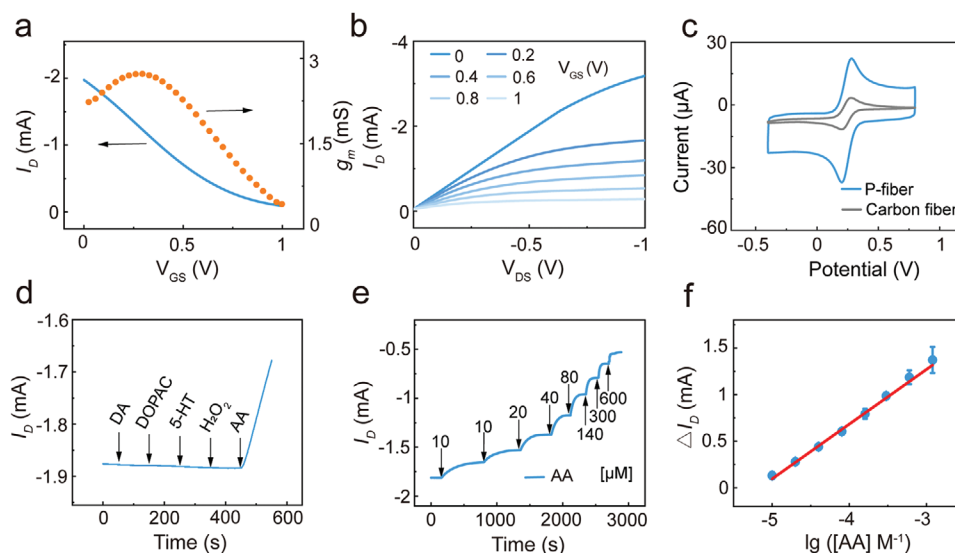


**Figure 2.** Electrochemical performance of PF-OECTs. a,b) Transfer curve and output curve of the PF-OECTs using artificial cerebrospinal fluid as the electrolyte, respectively. c) Cyclic voltammograms of P-fiber and carbon fiber obtained in the potassium ferricyanide solution. d) Drain current response toward the addition of 10 nM DA, 10 nM DOPAC, 10 nM 5-HT, 10  $\mu$ M H<sub>2</sub>O<sub>2</sub>, and 100  $\mu$ M AA. e) Drain current response toward the sequential addition of AA in the electrolyte. f) Plot of the drain current versus the logarithm of AA concentration.

## 2.2. Electrochemical Performance of PF-OECT

The volumetric capacitance and charge storage capacity of the P-fibers were first calculated from the cyclic voltammetry in 1x phosphate-buffered saline (1x PBS) with values of  $86.26 \pm 6.92 \text{ F cm}^{-3}$  and  $110.64 \pm 10.15 \text{ mC cm}^{-2}$ , respectively (Figure S7, Supporting Information). The high capacitive properties contributed to the performance of OECTs.<sup>[21]</sup> To evaluate the electrochemical performance of the PF-OECT, artificial cerebrospinal fluid was selected as the electrolyte (Figure S8, Supporting Information). The application of a positive gate voltage induces cations from the artificial cerebrospinal fluid to enter the channel and de-dope it, which is a reversible process.<sup>[5c]</sup> The transfer curve of the PF-OECT was tested with a drain voltage ( $V_{DS}$ ) of  $-0.6 \text{ V}$ , and a gate voltage ( $V_{GS}$ ) ranging from 0 to 1 V (Figure 2a). A maximal transconductance ( $g_m$ ) of 2.73 mS was obtained, which is comparable to most reported OECTs, ensuring efficient amplification for high sensitivity.<sup>[22]</sup> Furthermore, to characterize its ability to function as a transistor,  $V_{DS}$  was swept from 0 to  $-1 \text{ V}$  and  $V_{GS}$  was set at 0, 0.2, 0.4, 0.6, 0.8, and 1 V. The output curve was then plotted for decreasing drain current ( $I_D$ ) as  $V_{GS}$  increased (Figure 2b).

The electrochemical activity of the gate electrode is an important factor for the sensitivity of OECT.<sup>[23]</sup> Thus, it was characterized in a potassium ferricyanide solution. P-fibers demonstrated a larger peak current of cyclic voltammograms compared with the carbon fibers which were typically used as implantable electrodes (Figure 2c). Furthermore, the normalized areas (active surface area divided by geometric area) of both fibers were extracted from the cyclic voltammograms, which illustrated that P-fibers have larger normalized areas due to the porous structure with much more electrochemical reaction active sites (Figure S9, Supporting Information), benefiting for electrochemical activity even with a small size of electrode.<sup>[3b]</sup>

Next, we chose AA as an example to investigate the sensing abilities of the PF-OECTs. This is because AA is an important antioxidant and neuromodulator in the central nervous system and is linked to neurological diseases such as epilepsy.<sup>[24]</sup> Generally, AA is oxidized on the surface of the gate under the positive gate voltage (Figure S10, Supporting Information). The gate voltage is applied between the gate and channel and caused a drop across the electric double layers of the gate and channel.<sup>[25]</sup> The oxidation of AA on the gate leads to a higher voltage drop on the surface of the channel, which results in more cations entering into the channel and increasing the resistance of the channel and decreasing the drain current.<sup>[26]</sup> As a result, the change in AA concentration can be transduced into drain current signals. To prove the sensing properties of gate electrodes for AA, cyclic voltammograms at P-fibers were first evaluated in artificial cerebrospinal fluid containing AA, 3,4-dihydroxyphenylacetic acid (DOPAC), hydrogen peroxide (H<sub>2</sub>O<sub>2</sub>), dopamine (DA), and serotonin (5-HT) (Figure S11, Supporting Information). The oxidation potential of AA ( $\approx 0 \text{ V}$ ) was significantly lower than that of other electroactive chemicals ( $>0.1 \text{ V}$ ), and the presence of other electroactive chemicals did not reduce the AA signal. The peak current of AA remained stable after 50 cycles of scanning, indicating good repeatability. Therefore, the selective detection of AA could be achieved by carefully choosing the oxidation potential.<sup>[27]</sup> Accordingly, when the gate voltage of 0.2 V was applied, a more significant current change of PF-OECT to AA was observed compared to the aforementioned interferences under similar physiological concentrations (Figure 2d).

Therefore, a typical stepwise response to AA is shown in Figure 2e with the continuous addition of AA. A linear relationship was observed between the change in drain current and the logarithm of AA concentration in the range from 10 to 1200  $\mu$ M with good reproducibility (Figure 2f), demonstrating a sensitivity of  $0.587 \pm 0.017 \text{ mA } (\lg([\text{AA}] \text{ M}^{-1}))^{-1}$ . The high sensitivity of

PF-OECT to AA is due to the electrocatalytic effects of PEDOT and the in situ amplification capabilities of the OECT.<sup>[28]</sup>

### 2.3. Flexibility and Stability of PF-OECT

The P-fibers, as the main component of PF-OECT, were designed to be flexible and able to be wound or knotted around a transparent glass tube (Figure 3a). To simulate in vivo experiments, the P-fibers were implanted into 0.6 wt.% agar gels, which serve as a substitute for brain tissue, as illustrated in Figure 3b.<sup>[29]</sup> The gels were held in place by two glass sheets at the bottom and top. When the gels were compressed with a plastic tube in the middle, the P-fibers bent along with the gels without any gaps, demonstrating their high level of flexibility and ability to conform to deformations. The effective Young's modulus of the P-fibers was found to be  $3.15 \pm 0.05$  kPa (Figure 3c) via the nanoindentation method, which is

comparable to that of the brain tissue ( $3.02 \pm 0.13$  kPa). Additionally, fluorine rubber showed an effective Young's modulus of  $1.45 \pm 0.08$  MPa, which is similar to that of axons.<sup>[30]</sup> The mechanical compatibility between PF-OECT and brain tissue will help to establish a stable device-tissue interface.

As the brain arbitrarily moves and deforms in a physiological environment, we further studied the electrochemical performances of PF-OECTs under dynamic deformations, e.g., different-angle bending, cyclic bending and twisting. The transfer curve of PF-OECT, the normalized oxidation peak current and the impedance of the gate were all stable at increasing bending angles from  $0^\circ$  to  $180^\circ$ , and after 3000 cycles of bending with an angle of  $60^\circ$  and twisting with a torsion level of  $50 \text{ rad m}^{-1}$  (Figure 3d–h; Figure S12a–d, Supporting Information). Furthermore, to mimic the dynamic motion of the brain due to respiration and heartbeat, the PF-OECTs were tested at increasing dynamic frequencies from 0 to 10 Hz under mechanical stirring.<sup>[3b]</sup> There were also no obvious changes in the

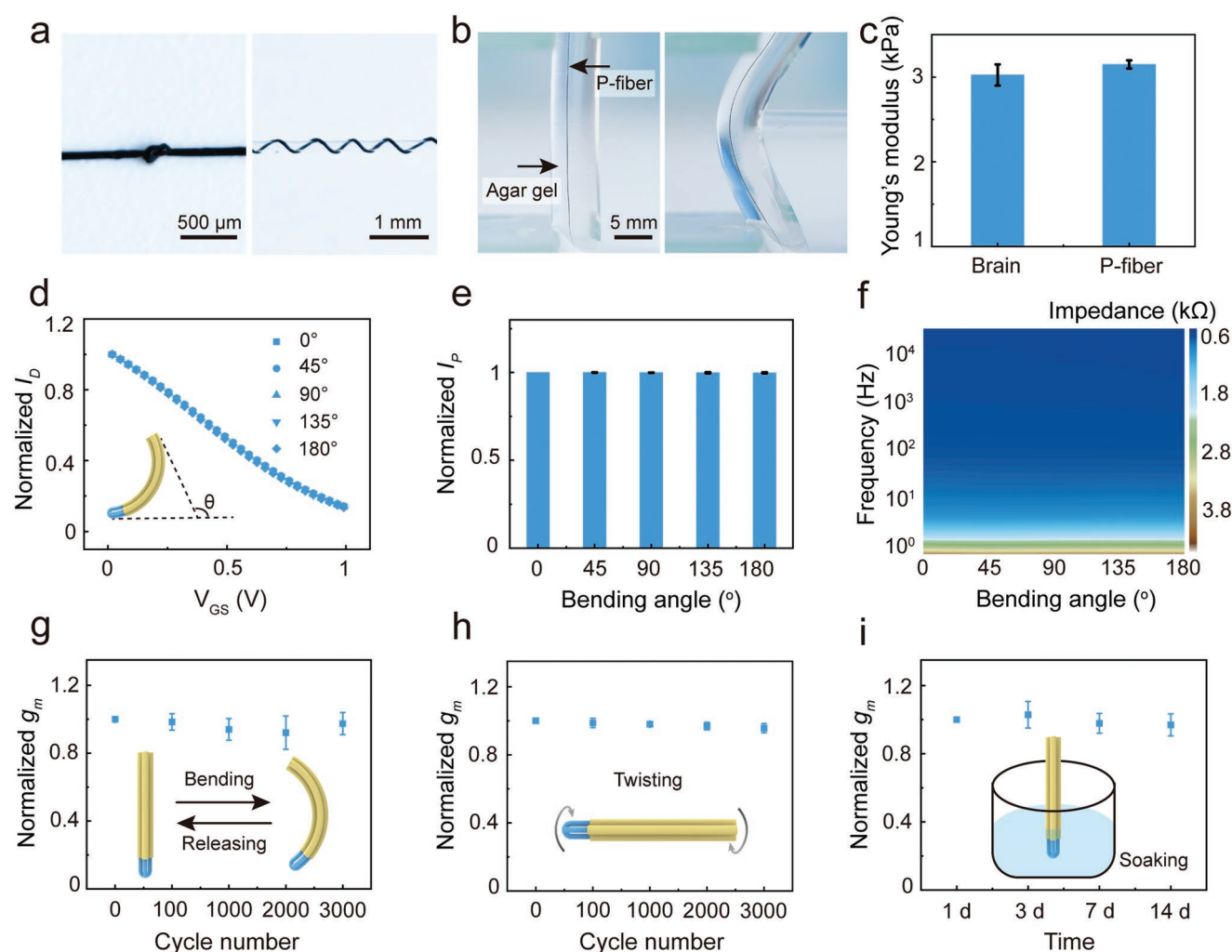


**Figure 3.** Flexibility and stability of PF-OECTs. a) Photographs of knotted P-fiber and P-fiber wound on the surface of a glass tube. b) Photographs of the agar gel implanted with P-fiber before and after a plastic tube pressing onto its middle part. c) Effective Young's modulus of P-fiber and brain tissue obtained via nanoindentation. d–f) Transfer curve of PF-OECT, normalized oxidation peak current and impedance of gate electrode tested under different bending angles in the potassium ferricyanide solution, respectively. g–i) Normalized transconductances of PF-OECT under bending for 3000 cycles, twisting for 3000 cycles, and immersed for 14 days in artificial cerebrospinal fluid, respectively.



normalized transconductance and impedance (Figure S12e,f, Supporting Information). Additionally, the PF-OECT was stable after immersing in artificial cerebrospinal fluid at 37 °C for 14 days (Figure 3i; Figure S12g,h, Supporting Information).

#### 2.4. Anti-Biofouling Performance of PF-OECT

In addition to flexibility and dynamic stability, the anti-biofouling performance is another critical parameter for electrochemical sensing in vivo.<sup>[31]</sup> Biofouling is a common issue that occurs after the implantation of electrodes, leading to protein corona formation around the implanted devices, hindering the mass transport of analytes from the electrolyte to the electrode surface.<sup>[10a,32]</sup> This process ultimately decreases the sensitivity of electrochemical sensors.<sup>[33]</sup> To evaluate the anti-biofouling performances of PF-OECTs, a 10 mg mL<sup>-1</sup> bovine

serum albumin (BSA) solution was used to simulate the environment in vivo (Figure 4a). The nonspecific protein adsorption of P-fibers was characterized by immersing them in fluorescein isothiocyanate-tagged BSA (FITC-BSA) solution for 2 h. The fluorescence image showed no significant protein fouling on the P-fibers (Figure 4b). In contrast, the carbon fibers demonstrated bright green fluorescence (Figure 4c), indicating obvious protein adsorption on their surface. The anti-biofouling capabilities of P-fibers probably can be ascribed to their hydrophilicity from the PSS component.<sup>[12]</sup> As shown in Figure 4d, the water contact angle of P-fibers was near 0°, much lower than 102.8° of carbon fibers (Figure 4e).

To further assess the anti-biofouling performance of PF-OECTs, the cyclic voltammograms of the gate were recorded before and after immersion in the BSA solutions for up to 14 days. The results showed that the curves remained nearly unchanged (Figure 4f), while the peak currents of the carbon

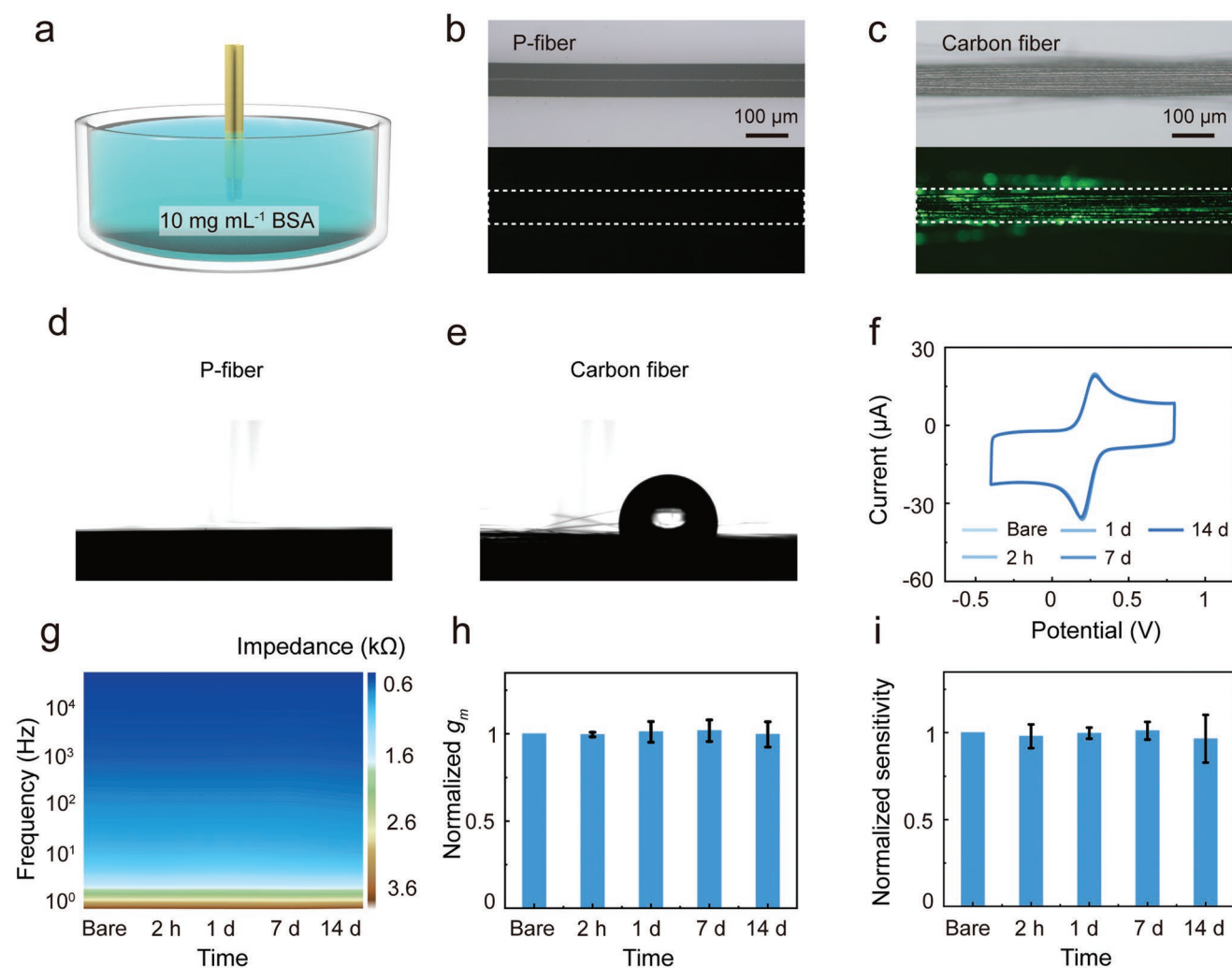


**Figure 4.** The anti-biofouling performance of PF-OECT. a) Schematic diagram of PF-OECT incubated in 10 mg mL<sup>-1</sup> BSA solution. b, c) Microscopy (top) and fluorescence microscopy images (bottom) of P-fiber and carbon fiber after incubation in FITC-BSA (green) solutions, respectively. d, e) The water contact angle test of P-fibers and carbon fibers, respectively. f) Cyclic voltammograms of gate electrode obtained in the potassium ferricyanide solution before (bare) and after incubation in 10 mg mL<sup>-1</sup> BSA solution for different time. g, h) Impedance of gate electrode and normalized transconductance of PF-OECTs after incubation in 10 mg mL<sup>-1</sup> BSA solution for different periods, respectively. i) Normalized sensitivity of PF-OECT to AA detection after incubation in 10 mg mL<sup>-1</sup> BSA solution for different periods.

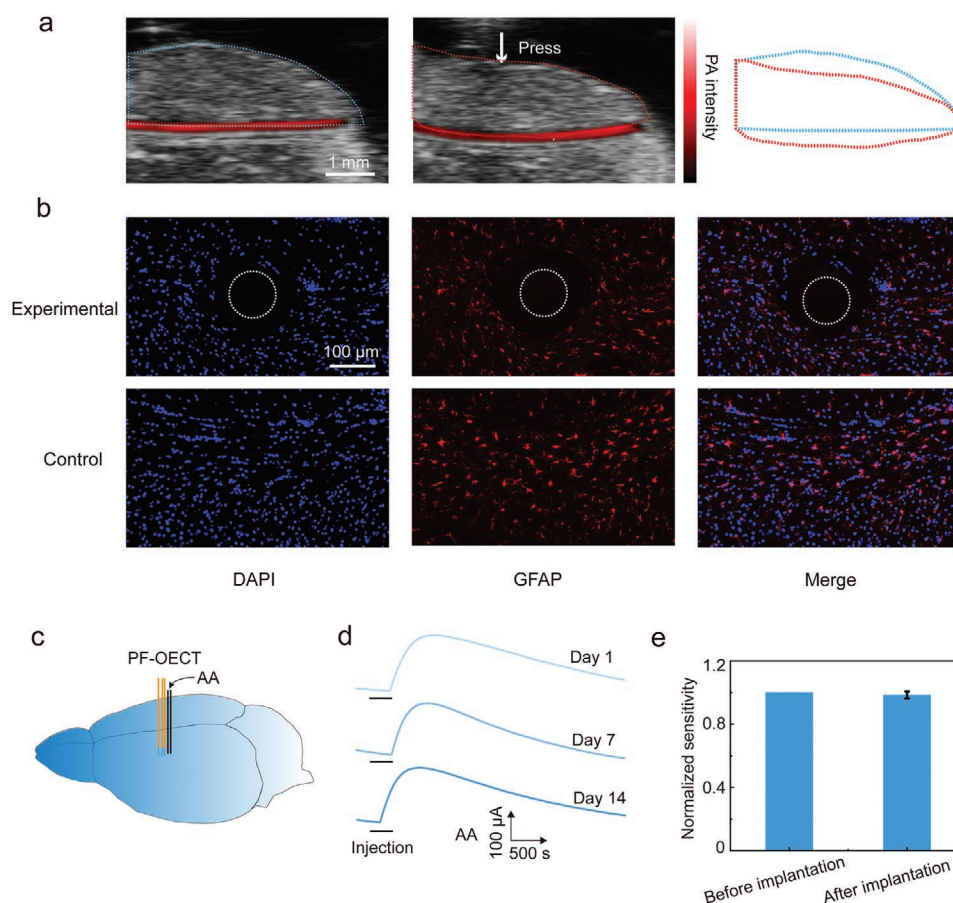


**Figure 5.** The performance and biocompatibility of PF-OECTs in mice brains. a) Photoacoustic (PA) images of a mouse brain with a PF-OECT before and after mechanical pressing. The right contour lines were drawn from the PA images. b) Immunohistochemical staining images of brain slices at 14 days after implantation of PF-OECT and control group without implants. Blue and red correspond to 4',6-diamidino-2-phenylindole (DAPI, label of cell nuclei) and glial fibrillary acidic protein (GFAP, label of astrocytes), respectively. The white dotted circle indicates the position of the PF-OECT. c) Schematic diagram of in vivo detection of AA with the PF-OECT. d) Real-time sensing of AA for 14 days toward locally injecting 2  $\mu\text{L}$  of 5 mM AA at a rate of 0.4  $\mu\text{L min}^{-1}$ . e) Normalized sensitivity of PF-OECT for AA before and after implantation in mouse brain for 14 days.

fibers decreased obviously after only 2 h of incubation and continued to decline over time (Figure S13, Supporting Information). The impedance of gate and normalized transconductance of PF-OECT remained stable with minor fluctuations both before and after incubation in BSA solutions for 14 days (Figure 4g,h). Finally, the normalized sensitivity (sensitivity divided by the sensitivity of PF-OECT before incubation in BSA solution) of PF-OECTs for AA was stable during the incubation period in BSA solution (Figure 4i), indicating its good anti-biofouling performance.

## 2.5. In Vivo Performance of PF-OECT

PF-OECTs were implanted into mice brains to study the dynamic interface between brain and device under deformation (Figure 5a). The photoacoustic (PA) imaging showed that the PF-OECT bent along with the mouse brain under compression, demonstrating that the device was flexible enough to form a stable interface with the brain. Immunohistochemical staining was used to characterize the cell distribution around PF-OECT after implanting in the mouse brain for 14 days (Figure 5b;

Figure S14, Supporting Information). Specifically, the cell nuclei, astrocytes and microglia were stained by 4',6-diamidino-2-phenylindole (DAPI), glial fibrillary acidic protein (GFAP), and ionized calcium-binding adapter molecule (Iba-1), respectively. The results demonstrated that there were no significant differences in the expression of DAPI, GFAP and Iba-1 between the experimental and control groups, indicating high biocompatibility of PF-OECTs.

Taking advantages of their flexibility, anti-biofouling capability and biocompatibility, PF-OECTs have the potential to be used for long-term chemical monitoring in the brain. To test this, the PF-OECT was implanted into the mouse brain with the help of a stereotaxic apparatus (Figure 5c). After the implantation, the mouse was still active and the PF-OECT appeared like the hair of the mouse (Figure S15, Supporting Information). Then, 2  $\mu\text{L}$  of 5 mM AA solution was injected into the brain via intracerebral microperfusion pipette, positioned 100  $\mu\text{m}$  away from the PF-OECT to avoid mechanical interference. As a result of concentration diffusion and cerebrospinal fluid circulation, the AA approached the PF-OECT gradually. This was accompanied by the gradual appearance of a current peak, recorded by the PF-OECT, while there was

no noticeable change when the AA solution was replaced with saline (Figure S16, Supporting Information). This demonstrated that the current peak was caused by AA rather than physical diffusion force. In addition, the specificity of PF-OECT *in vivo* has been measured, which showed that the current signal was not obviously disturbed by other chemicals (Figure S17, Supporting Information). The PF-OECTs were maintained in the brain for 14 days, with AA solutions being injected into the mouse brain every several days, and showed similar current peaks each time (Figure 5d). Moreover, the normalized sensitivities (sensitivity divided by the sensitivity before implantation) of PF-OECT showed only a minor decline after 14 days in the brain (Figure 5e). Compared to most reported AA electrochemical sensors, which have a working time of less than one day, the PF-OECT demonstrated 14-day stable detection in the mouse brain (Table S1, Supporting Information), illustrating its potential as a chronic implantable electrochemical sensor.

### 3. Conclusion

In summary, a high-flexibility, anti-biofouling PF-OECT has been developed using all-polymer materials. The *in situ* amplification endows the PF-OECT with higher sensitivity. The intrinsic softness and flexibility of the PF-OECT ensured a stable mechanical and electrochemical interface with the soft brain tissue, even under repeated deformation. The hydrophilic PEDOT:PSS provides good anti-biofouling properties, resulting in high sensitivity retention in BSA solution. After being implanted into a mouse brain, the PF-OECT demonstrated high biocompatibility and stable AA monitoring for 14 days. This all-polymer fiber design strategy can be expanded to create more flexible and anti-biofouling electrochemical sensors by using different soft, biocompatible polymers with additional functions, providing a promising platform for developing implantable electronics.

### 4. Experimental Section

**Materials:** Poly(3,4-ethylene dioxythiophene):poly(styrene sulfonate) (PEDOT:PSS) aqueous dispersion (Clevios PH1000) was purchased from Heraeus. Sodium alginate, bovine serum albumin (BSA), 5-Hydroxytryptamine Hydrochloride and dodecyl benzene sulfonic acid were ordered from Sigma Aldrich Co. Ascorbic acid (AA) and agarose were purchased from Aladdin Reagent Database Inc. Dopamine hydrochloride and 3,4-dihydroxyphenylacetic acid were purchased from Damas-beta. Artificial cerebrospinal fluid was purchased from Leagene Biotechnology. Fluorescein isothiocyanate-tagged bovine serum albumin (FITC-BSA) was obtained from Solarbio Science and Technology Co., Ltd. Carbon fibers were provided by Toray Industries, Inc. Dental cements were purchased from Nissin Dental Products Inc. All other common reagents were purchased from Sinopharm Chemical Reagent Co., Ltd.

**Fabrication of PEDOT:PSS Fibers (P-Fibers):** Deionized water was added to the sodium alginate powder, followed by stirring overnight at room temperature to obtain the sodium alginate solution with a concentration of 2 wt.%. Air bubbles were eliminated from the above solution through a vacuum oven at room temperature. 0.5 wt.% calcium chloride solutions were prepared by adding calcium chloride particles to deionized water and shaking until the solution became clear and transparent. For the preparation of PEDOT:PSS solution, dimethyl sulfoxide (5 v/v%) was added to the PEDOT:PSS aqueous

dispersion (solid content of 1%), followed by 10 min of vortex. Dodecyl benzenesulfonic acid (3.5 v/v%) was then mixed with the above solution, followed by 1 min of the vortex and 2 min of centrifugation at a speed of 11 000 r min<sup>-1</sup>. The fabrication of P-fibers was through a specially made three-channel spinneret and could be separated into two steps. First, the PEDOT:PSS solution was extruded from two parallel channels, while the sodium alginate solution was extruded from the other channel of the same spinneret, followed by entering the coagulation bath of 0.5 wt.% calcium chloride solutions. Generally, to promise the laminar flow, the flow rates of the PEDOT:PSS solutions and the sodium alginate solutions were 180 μL min<sup>-1</sup> and 1500 μL min<sup>-1</sup>, respectively. Second, P-fibers were removed from the alginate hydrogel via mechanical force and rinsed thoroughly with 1x PBS and deionized water.

**Fabrication of All-Polymer Organic Electrochemical Transistors (PF-OECTs):** Dry the P-fibers at room temperature. Fluorine rubber was mixed with 4-methyl 2-pentanone and stirred at 80 °C for 1 day, followed by 10 min of centrifugation at a speed of 14 000 r min<sup>-1</sup>. The fluorine rubber was 10 wt.% in the resulting viscous, transparent solution. For the insulating process to produce channel, the two ends of P-fibers were fixed on a hollow polyethylene terephthalate (PET) plate using polyimide tape. One end of the PET plate was fixed on the stereotaxic apparatus and immersed in 10 wt.% insulating fluorine rubbers steadily for seconds, then pulled out quickly with the help of the stereotaxic apparatus and dried for several minutes. The immersing and pulling cycle were repeated for 5 times. Then, the above operation was repeated on the other end of PET plate. The above fibers were hung for 2 days to eliminate the solvent fully. Then the insulated fiber was folded with the channel part as the folding point under the microscope to ensure reliability. Finally, the folded channel fiber was assembled with gate fiber to form the PF-OECT.

**Characterization:** Photographs were taken using a digital camera (SONY A6000, Japan). Optical microscopy images were taken by Olympus EX51. Zeiss Gemini SEM500 FESEM was used to obtain the scanning electron microscopy (SEM) images. Rheological properties were obtained via a rotational rheometer (ThermoFisher HAAKE MARS III). X-ray photoelectron spectroscopy (XPS) was acquired by a scanning XPS Microprobe (Thermo Scientific K-Alpha+) using a micro-focused monochromator Al K-alpha X-ray source. Raman spectroscopy was performed using Renishaw InVia Qontor equipped with an Ar ion laser with 532 nm excitation wavelength at 5% laser power. Conductivity was measured by a Keithley 2400 source meter with a four-point probe method. The electrochemical characterizations of PF-OECT were characterized by a CHI660e electrochemical workstation and Keithley 2400 source meter, where the gate and source electrodes were connected to the Keithley 2400 source meter, the drain and source electrodes were connected to the CHI660e electrochemical workstation. The P-fibers, platinum wire and Ag/AgCl were chosen as the working, counter and reference electrodes, respectively. The cyclic voltammograms (CV) were characterized at a voltage range from -0.4 to 0.8 V at a scan rate of 50 mV s<sup>-1</sup> if the conditions were not pointed out especially. Charge storage capacity was obtained from the time integral of the cathodic current in CV. The volumetric capacitance was calculated from CV based on the following equations:<sup>[34]</sup>

$$C_V = \frac{1}{2\nu\Delta U} \int I(U) dU \quad (1)$$

Where  $C_V$  is the volumetric capacitance in F cm<sup>-3</sup>,  $\nu$  is the scan rate in V s<sup>-1</sup>,  $V$  is the volume in cm<sup>3</sup>,  $\Delta U$  is the potential range in V,  $I(U)$  is the instantaneous current in CV curves and  $U$  is applied voltage in V. Electrochemical impedance spectroscopy was obtained using A.C. impedance parameters within a frequency range from 1 to 100 000 Hz. Static water contact angles were characterized using a contact angle goniometer to study the hydrophilicity of P-fibers and carbon fibers. Nanoindentation tests for the P-fibers and brain were performed through a Piuma Nanoindenter (Optics 11 BV) with a spherical indenter with a diameter of 10 μm and stiffness of 0.48 N m<sup>-1</sup>, followed by 2 s loading and 1 s holding. The effective Young's moduli were calculated according



to the Hertz model. To study the protein adsorption, P-fibers and the carbon fibers were incubated in 1 mg mL<sup>-1</sup> FITC-BSA for 2 h. Then the fibers were washed using deionized water thoroughly, followed by fluorescence imaging performed on Olympus EX51. The photoacoustic images were obtained and analyzed through a Vevo LAZR Imaging System (Fuji Film Visual Sonics Inc).

**In Vivo Monitoring of Ascorbic Acid:** The animal experiment protocols were approved by the Animal Experimentation Committee of Fudan University. All animals were treated in terms of guidelines for the care and use of experimental animals described by the National Institutes of Health and Fudan University (approval number: SYXK2020-0032). Male mice (ICR, 5 weeks old, Shanghai SLAC Laboratory Animal Co., Ltd.) were kept at controlled temperature and humidity. The mice were anesthetized with 1.5% isoflurane. The PF-OECTs were carefully implanted with the tungsten wire-assisted method through stereotaxic apparatus (RWD Life Science Co., Ltd.). To avoid the electrical short circuit, the gate and channel were separated from 100 μm. After implantation, the mice were taken from the stereotaxic apparatus and treated carefully. The monitoring of AA started from the second day after the implantation of PF-OECT. 2 μL 5 mM AA solution and 0.9% NaCl solution were injected by a glass microtube (inner diameter: 50 μm) using quintessential stereotaxic injector (Stoelting Co. 53 311) at a velocity of 0.4 μL min<sup>-1</sup>. The site of glass microtube was near the PF-OECT ≈100 μm distance to avoid the mechanical disturbance. All conditions were the same except for the components of solutions between the experimental and control group. For the chronic detection of AA in the mouse brain, the PF-OECT was fixed on the skull via dental cement.

**Immunofluorescence Staining:** Mice were sacrificed after PF-OECTs implanted for 14 days, followed by the removal of brains. The brains were fixed with 4 v% paraformaldehyde solution and then cut into slices with thicknesses of 4 μm by a microtome (Leica RM2016, Leica Microsystems). Next, antigen retrieval was performed via heating in 10 mM citrate buffer (pH 6.0) of a microwave oven at ≈400 W for 8 min and at ≈240 W for 7 min after a break for 8 min. Rabbit anti-gial fibrillary acidic protein (1:500, GB11096, Servicebio) and rabbit anti-ionized calcium-binding adapter molecule-1 (1:500, GB13105, Servicebio) were used as primary antibodies. Cy3 conjugated goat anti-rabbit IgG (H+L) (1:300, GB21303, Servicebio) and Alexa Fluor® 488-conjugated goat anti-mouse IgG (H+L) (1:500, GB23303, Servicebio) were used as secondary antibodies. The cell nuclei were stained by 4',6-diamidino-2-phenylindole (G1012, Servicebio). The immunofluorescence-stained sections were observed with Panoramic MIDI (3DHISTECH Ltd.).

## Supporting Information

Supporting Information is available from the Wiley Online Library or from the author.

## Acknowledgements

This work was supported by NSFC (52122310, 22075050), STCSM (21511104900, 20JC1414902), Shanghai Municipal Science and Technology Major Project (2018SHZDZX01), ZJ Lab, and Shanghai Center for Brain Science and Brain-Inspired Technology.

## Conflict of Interest

The authors declare no conflict of interest.

## Data Availability Statement

The data that support the findings of this study are available from the corresponding author upon reasonable request.

## Keywords

all-polymers, fiber organic electrochemical transistors, flexibility, anti-biofouling, ascorbic acid

Received: December 23, 2022

Revised: March 18, 2023

Published online: April 16, 2023

- [1] a) K. T. Kishida, I. Saez, T. Lohrenz, M. R. Witcher, A. W. Laxton, S. B. Tatter, J. P. White, T. L. Ellis, P. E. M. Phillips, P. R. Montague, *Proc. Natl. Acad. Sci. USA* **2016**, *113*, 200; b) N. Nakatsuka, K.-A. Yang, J. M. Abendroth, K. M. Cheung, X. Xu, H. Yang, C. Zhao, B. Zhu, Y. S. Rim, Y. Yang, P. S. Weiss, M. N. Stojanović, A. M. Andrews, *Science* **2018**, *362*, 319; c) T. Patriarchi, J. R. Cho, K. Merten, M. W. Howe, A. Marley, W.-H. Xiong, R. W. Folk, G. J. Broussard, R. Liang, M. J. Jang, H. Zhong, D. Dombeck, M. von Zastrow, A. Nimmerjahn, V. Gradinaru, J. T. Williams, L. Tian, *Science* **2018**, *360*, eaat4422.
- [2] a) L. Wang, S. Xie, Z. Wang, F. Liu, Y. Yang, C. Tang, X. Wu, P. Liu, Y. Li, H. Saiyin, S. Zheng, X. Sun, F. Xu, H. Yu, H. Peng, *Nat. Biomed. Eng.* **2020**, *4*, 159; b) J. Li, Y. Liu, L. Yuan, B. Zhang, E. S. Bishop, K. Wang, J. Tang, Y.-Q. Zheng, W. Xu, S. Niu, L. Beker, T. L. Li, G. Chen, M. Diyaolu, A.-L. Thomas, V. Mottini, J. B. H. Tok, J. C. Y. Dunn, B. Cui, S. P. Paşca, Y. Cui, A. Habtezion, X. Chen, Z. Bao, *Nature* **2022**, *606*, 94; c) C. Chen, J. Feng, J. Li, Y. Guo, X. Shi, H. Peng, *Chem. Rev.* **2023**, *123*, 613.
- [3] a) M. Labib, E. H. Sargent, S. O. Kelley, *Chem. Rev.* **2016**, *116*, 9001; b) X. Wu, J. Feng, J. Deng, Z. Cui, L. Wang, S. Xie, C. Chen, C. Tang, Z. Han, H. Yu, X. Sun, H. Peng, *Sci. China Chem.* **2020**, *63*, 1281.
- [4] a) J. Rivnay, S. Inal, A. Salleo, R. M. Owens, M. Berggren, G. G. Malliaras, *Nat. Rev. Mater.* **2018**, *3*, 17086; b) J. Fan, A. A. Forero Pico, M. Gupta, *Mater. Adv.* **2021**, *2*, 7445.
- [5] a) C. Liao, C. Mak, M. Zhang, H. L. W. Chan, F. Yan, *Adv. Mater.* **2015**, *27*, 676; b) H. Tang, F. Yan, P. Lin, J. Xu, H. L. W. Chan, *Adv. Funct. Mater.* **2011**, *21*, 2264; c) A. Nawaz, Q. Liu, W. L. Leong, K. E. Fairfull-Smith, P. Sonar, *Adv. Mater.* **2021**, *33*, 2101874.
- [6] a) W. Li, J. Jin, T. Xiong, P. Yu, L. Mao, *Angew. Chem., Int. Ed.* **2022**, *61*, 202204134; b) K. Xie, N. Wang, X. Lin, Z. Wang, X. Zhao, P. Fang, H. Yue, J. Kim, J. Luo, S. Cui, F. Yan, P. Shi, *eLife* **2020**, *9*, 50345.
- [7] a) I. Terem, W. W. Ni, M. Goubran, M. S. Rahimi, G. Zaharchuk, K. W. Yeom, M. E. Moseley, M. Kurt, S. J. Holdsworth, *Magn. Reson. Med.* **2018**, *80*, 2549; b) K. C. Spencer, J. C. Sy, K. B. Ramadi, A. M. Graybiel, R. Langer, M. J. Cima, *Sci. Rep.* **2017**, *7*, 1952; c) H. N. Schwerdt, M. J. Kim, S. Amemori, D. Homma, T. Yoshida, H. Shimazu, H. Yerramreddy, E. Karasan, R. Langer, A. M. Graybiel, M. J. Cima, *Lab Chip* **2017**, *17*, 1104.
- [8] a) J. Feng, C. Chen, X. Sun, H. Peng, *Acc. Mater. Res.* **2021**, *2*, 138; b) X. Liu, T. Xiao, F. Wu, M.-Y. Shen, M. Zhang, H.-h. Yu, L. Mao, *Angew. Chem., Int. Ed.* **2017**, *56*, 11802.
- [9] a) C. Jiang, G. Wang, R. Hein, N. Liu, X. Luo, J. J. Davis, *Chem. Rev.* **2020**, *120*, 3852; b) A. Barfidokht, J. J. Gooding, *Electroanalysis* **2014**, *26*, 1182; c) D. L. Elbert, J. A. Hubbell, *Annu. Rev. Mater. Sci.* **1996**, *26*, 365.
- [10] a) Y.-L. Liu, W.-H. Huang, *Angew. Chem., Int. Ed.* **2021**, *60*, 2757; b) H.-R. Lim, H. S. Kim, R. Qazi, Y.-T. Kwon, J.-W. Jeong, W.-H. Yeo, *Adv. Mater.* **2020**, *32*, 1901924.
- [11] T. D. Y. Kozai, N. B. Langhals, P. R. Patel, X. Deng, H. Zhang, K. L. Smith, J. Lahann, N. A. Kotov, D. R. Kipke, *Nat. Mater.* **2012**, *11*, 1065.
- [12] L. V. Kayser, D. J. Lipomi, *Adv. Mater.* **2019**, *31*, 1806133.
- [13] W. Zhang, Z. Su, X. Zhang, W. Wang, Z. Li, *VIEW* **2022**, *3*, 20220030.
- [14] B. Lu, H. Yuk, S. Lin, N. Jian, K. Qu, J. Xu, X. Zhao, *Nat. Commun.* **2019**, *10*, 1043.



- [15] S. Zhang, Y. Chen, H. Liu, Z. Wang, H. Ling, C. Wang, J. Ni, B. Çelebi-Saltik, X. Wang, X. Meng, H.-J. Kim, A. Baidya, S. Ahadian, N. Ashammakhi, M. R. Dokmeci, J. Travas-Sejdic, A. Khademhosseini, *Adv. Mater.* **2020**, *32*, 1904752.
- [16] M. Liao, C. Wang, Y. Hong, Y. Zhang, X. Cheng, H. Sun, X. Huang, L. Ye, J. Wu, X. Shi, X. Kang, X. Zhou, J. Wang, P. Li, X. Sun, P. Chen, B. Wang, Y. Wang, Y. Xia, Y. Cheng, H. Peng, *Nat. Nanotechnol.* **2022**, *17*, 372.
- [17] C. Tang, S. Xie, M. Wang, J. Feng, Z. Han, X. Wu, L. Wang, C. Chen, J. Wang, L. Jiang, P. Chen, X. Sun, H. Peng, *J. Mater. Chem. B* **2020**, *8*, 4387.
- [18] Y. Liu, J. Liu, S. Chen, T. Lei, Y. Kim, S. Niu, H. Wang, X. Wang, A. M. Foudeh, J. B. H. Tok, Z. Bao, *Nat. Biomed. Eng.* **2019**, *3*, 58.
- [19] J. Ouyang, C. W. Chu, F. C. Chen, Q. Xu, Y. Yang, *Adv. Funct. Mater.* **2005**, *15*, 203.
- [20] a) J. Liu, Y. Jia, Q. Jiang, F. Jiang, C. Li, X. Wang, P. Liu, P. Liu, F. Hu, Y. Du, J. Xu, *ACS Appl. Mater. Interfaces* **2018**, *10*, 44033; b) R. Jalili, J. M. Razal, P. C. Innis, G. G. Wallace, *Adv. Funct. Mater.* **2011**, *21*, 3363.
- [21] J. Rivnay, P. Leleux, M. Ferro, M. Sessolo, A. Williamson, D. A. Koutsouras, D. Khodagholy, M. Ramuz, X. Strakosas, R. M. Owens, C. Benar, J.-M. Badier, C. Bernard, G. G. Malliaras, *Sci. Adv.* **2015**, *1*, 1400251.
- [22] a) H. Lee, S. Lee, W. Lee, T. Yokota, K. Fukuda, T. Someya, *Adv. Funct. Mater.* **2019**, *29*, 1906982; b) O. Parlak, S. T. Keene, A. Marais, V. F. Curto, A. Salleo, *Sci. Adv.* **2018**, *4*, eaar2904.
- [23] a) C. H. Mak, C. Liao, Y. Fu, M. Zhang, C. Y. Tang, Y. H. Tsang, H. L. W. Chan, F. Yan, *J. Mater. Chem. C* **2015**, *3*, 6532; b) L. Kergoat, B. Piro, D. T. Simon, M.-C. Pham, V. Noël, M. Berggren, *Adv. Mater.* **2014**, *26*, 5658.
- [24] H. Cheng, L. Li, M. Zhang, Y. Jiang, P. Yu, F. Ma, L. Mao, *TrAC, Trends Anal. Chem.* **2018**, *109*, 247.
- [25] A. Yang, Y. Li, C. Yang, Y. Fu, N. Wang, L. Li, F. Yan, *Adv. Mater.* **2018**, *30*, 1800051.
- [26] a) D. A. Bernards, G. G. Malliaras, *Adv. Funct. Mater.* **2007**, *17*, 3538; b) D. A. Bernards, D. J. Macaya, M. Nikolou, J. A. DeFranco, S. Takamatsu, G. G. Malliaras, *J. Mater. Chem.* **2008**, *18*, 116.
- [27] L. Xiang, P. Yu, J. Hao, M. Zhang, L. Zhu, L. Dai, L. Mao, *Anal. Chem.* **2014**, *86*, 3909.
- [28] a) I. Gualandi, E. Scavetta, F. Mariani, D. Tonelli, M. Tessarolo, B. Fraboni, *Electrochim. Acta* **2018**, *268*, 476; b) I. Gualandi, M. Marzocchi, E. Scavetta, M. Calienni, A. Bonfiglio, B. Fraboni, *J. Mater. Chem. B* **2015**, *3*, 6753.
- [29] Z.-J. Chen, G. T. Gillies, W. C. Broaddus, S. S. Prabhu, H. Fillmore, R. M. Mitchell, F. D. Corwin, P. P. Fatouros, *J. Neurosurg.* **2004**, *101*, 314.
- [30] X. Yang, T. Zhou, T. J. Zwing, G. Hong, Y. Zhao, R. D. Viveros, T.-M. Fu, T. Gao, C. M. Lieber, *Nat. Mater.* **2019**, *18*, 510.
- [31] a) J. Xu, H. Lee, *Chemosensors* **2020**, *8*, 66; b) J. Sabaté del Río, O. Y. F. Henry, P. Jolly, D. E. Ingber, *Nat. Nanotechnol.* **2019**, *14*, 1143.
- [32] a) X. Xie, J. C. Doloff, V. Yesilyurt, A. Sadraei, J. J. McGarrigle, M. Omami, O. Veisoh, S. Farah, D. Isa, S. Ghani, I. Joshi, A. Vegas, J. Li, W. Wang, A. Bader, H. H. Tam, J. Tao, H.-j. Chen, B. Yang, K. A. Williamson, J. Oberholzer, R. Langer, D. G. Anderson, *Nat. Biomed. Eng.* **2018**, *2*, 894; b) S. P. Nichols, A. Koh, W. L. Storm, J. H. Shin, M. H. Schoenfish, *Chem. Rev.* **2013**, *113*, 2528.
- [33] T. Xiao, F. Wu, J. Hao, M. Zhang, P. Yu, L. Mao, *Anal. Chem.* **2017**, *89*, 300.
- [34] H. Sheng, J. Zhou, B. Li, Y. He, X. Zhang, J. Liang, J. Zhou, Q. Su, E. Xie, W. Lan, K. Wang, C. Yu, *Sci. Adv.* **2021**, *7*, eabe3097.